

Reactive Inkjet Printing of Biocompatible Enzyme Powered Silk Micro-Rockets

David A. Gregory, Yu Zhang, Patrick J. Smith, Xiubo Zhao,* and Stephen J. Ebbens*

Production of small-scale devices that can autonomously generate thrust via catalytic reactions within fluidic environments has become an increasingly active field of research over the last ten years.^[1–3] Recently, this has led to a focus on potential applications^[4] including environmental monitoring and remediation,^[5–7] in vivo drug delivery and repair,^[8] and lab on a chip diagnostics.^[9] Here, we present inkjet printing as a means to realizing these envisaged goals, and as an alternative to the current time-consuming lab scale lithographic fabrication processes. The conventional lithographic approach to control the shape and material distribution within small-scale devices places significant limits on scalability and prevents responsive design and testing. Instead, we show here how embracing advances in printable materials and printing technology can allow rapid, scalable manufacture of digitally defined “micro-rocket” devices, which by virtue of the use of a silk scaffold show promising biocompatibility suggesting suitability for a wide range of future applications.

In order to produce effective propulsion from catalytic reactions, controlling the distribution of catalytic material relative to the shape of the device is a key challenge.^[10] For catalytic motors moved by phoretic phenomena, an asymmetric distribution of catalyst is essential,^[2,11] while for motors moved by momentum transfer during gas bubble detachment,^[12] controlling catalyst location improves directionality.^[10] Making devices with the required distribution of catalyst is difficult, and to date has often relied on time-consuming and expensive methods. For example, many devices use platinum metal

as the motion producing catalyst, due to its straightforward room temperature decomposition of hydrogen peroxide fuel, which rapidly evolves oxygen facilitating motion either by bubble nucleation and release, or by establishing a dissolved oxygen gradient. However, patterning platinum to produce useful directed motion requires access to vacuum evaporation equipment.^[3,13] In other examples, where enzymatic catalysts have been investigated, such as catalase, which also performs rapid peroxide decomposition, these have often been bound to evaporated metals using time-consuming chemical functionalization steps.^[14–16] Devices that perform functions such as attaching cargo,^[6] require additional spatially well-defined chemical functionalization, distributed so as not to interfere with the catalytic activity responsible for generating motion. There have also recently been a variety of different biocompatible micromotors reported that use enzymes but once again the production of these devices is highly complex.^[17] Again, using conventional approaches to achieve the desired compositional control for many different components is laborious. And, because of the significant effort needed to produce a given device structure, the rapid design and testing of different material configurations with varied shapes, sizes, and compositions has not been possible, hampering development for applications. Recent attempts to establish alternative routes for swimming device manufacture recognized these challenges, and deployed screen printing to manufacture platinum powered swimming devices with a range of shapes and sizes.^[18,19] However, these demonstrations still require the production of physical masks or an advanced digital micro-mirror device.^[19] The scale of the screen printed “fish” using physical masks was much larger than that achievable by state-of-the-art inkjet printing methods,^[18,20] where features smaller than 10 μm have been reported.^[21] In the case of optical printing^[19] device manufacture relied on UV-curable inks, and manual exchange of solutions to enable composition to be varied.

A further issue with the existing surface modification approach to producing catalytic motors is the propensity for surface fouling and loss of activity. For example, platinum catalytic activity is highly sensitive to surface contaminants such as hydrocarbons^[22] and thiols,^[23] and is also reduced by surface absorption of constituents of bio-fluids, reducing biocompatibility. Therefore, undesirable surfactant additives are required for many bubble-propelled platinum systems^[24] to reduce this fouling behavior.^[25] This focus on surface attachment has extended to examples where enzymes have been used in place of metallic catalysts, limiting catalytic activity to an enzyme monolayer.

D. A. Gregory, Y. Zhang, Dr. X. Zhao, Dr. S. J. Ebbens
Department of Chemical and Biological Engineering
University of Sheffield
Sheffield, Mappin Street S1 3JD, UK
E-mail: xiubo.zhao@sheffield.ac.uk;
s.ebbens@sheffield.ac.uk



Dr. P. J. Smith
Department of Mechanical Engineering
University of Sheffield
Sheffield, 64 Garden Street S1 4BJ, UK

Dr. X. Zhao
School of Pharmaceutical Engineering and Life Science
Changzhou University
Changzhou 213164, China

This is an open access article under the terms of the Creative Commons Attribution License, which permits use, distribution and reproduction in any medium, provided the original work is properly cited.

DOI: 10.1002/sml.201600921

Against this background, here we show, for the first time, that it is instead possible to generate rapidly moving bubble-propulsive micro-rockets by reactive inkjet printing^[26] of silk fibroin (SF) derived ink mixed with the propulsion generating enzyme (catalase). The use of an enzyme instead of the platinum particles deployed for the demonstrations of printed swimmers discussed above provides the potential for improved biocompatibility. SF is a versatile material due to its strong mechanical properties,^[27] excellent biocompatibility,^[28] adaptable biodegradability,^[29] and easy processing.^[30] It is an FDA approved biomaterial and has been used for many biomedical applications.^[31] SF has three different conformations, or polymorphs. Silk I is water soluble (random coil), Silk II is the state which consists of β -sheet secondary structure (spun silk state), and Silk III is an air/water assembled interfacial silk consisting of a helical structure.^[31,32] Secreted silk (Silk II) is commonly processed into water soluble regenerated silk fibroin (RSF) (Silk I) to allow printing. However, this means that a further conversion stage is required to convert the printed material back into a water insoluble rigid scaffold, such a step is clearly required here to manufacture solid micro-rockets. Exposing Silk I to chemicals such as methanol or potassium chloride, heat, or shear stress converts it to a β -sheet secondary structure (Silk II) and this phenomenon has been widely used to make silk scaffolds for different biomedical applications.^[31] Inkjet printing of differently doped silk inks has recently been shown to be effective for applications such as sensing bacterial contamination^[33] and bacterial hosting.^[34] It has also been reported that printed silk structures can significantly retain the activity of enzymes (e.g., horse radish peroxidase), making it an attractive choice of scaffold.^[33] However, in these examples, the structures formed were very thin and remained bound to a substrate and so full conversion to Silk II was not required (in one study partial conversion due to the shear stress involved during printing was suggested).^[34] Here, in order to ensure a rigid detachable scaffold we instead for the first time employ reactive inkjet printing (RIJ) to allow chemical treatment with methanol to the Silk II form. RIJ is a method of allowing two different ink solutions to react together to generate a new compound, or alternatively as in the deployment we use here, to produce a change in polymorphic form.^[26]

RIJ also shares the advantages of conventional inkjet printing to allow the straightforward manufacture of 3D objects with well-controlled shape and size, for example, by utilizing a layer-by-layer approach.^[35] Here we show that alternate printing of silk ink and methanol (which triggers the conformation change from soluble Silk I to insoluble Silk II)^[30,31,36] allows the manufacture of propulsive micro-rockets with digitally defined size, shape, and catalyst distribution. We subsequently use the straightforward ability to vary micro-rocket catalyst distribution to compare trajectories from micro-rockets in which the entire structure incorporates catalase (which is capable of nucleating propulsion-generating oxygen bubbles), with those where only a specific segment of the structure/rocket contains enzyme. This comparison demonstrates the importance of spatial control and that confining the catalyst to one part of the structure produces well-defined linear trajectories, as opposed to the

chaotic motion produced from a homogeneous rocket. Furthermore, we demonstrate that by incorporating the catalyst throughout the micro-rockets' porous structure (Figure S1, Supporting Information) in the active segment, rather than only at the surface, enzyme stability is maintained for long durations. In addition, enzyme activity (catalase) is retained even in low pH environments (pH \approx 4), in contrast the same enzyme in free solution lost 90% activity after only 10 min in the same fuel solution. This is most likely due to the silk scaffold enhancing the enzyme stability and retaining its activity as has been previously reported by others.^[37] These advantages afforded by the use of a silk scaffold consequently lead to improved biocompatibility when compared to similar previous devices, and allow propulsion within bio fluids without the requirement for surfactant additives. Due to the remarkable potential for silk based materials^[30,31] in applications such as drug delivery^[38,39] and as a scaffold material^[40] for tissue engineering^[41] as well as for enzyme immobilisation,^[33,42] evidenced by much recent research attention, the future potential to further develop these micro-rockets is significant. Thus, for example, use of alternative motion producing enzymes that do not require hydrogen peroxide fuel, can easily be envisaged,^[15] and the incorporation of bio-recognition elements such as antibodies in specific regions of the micro-rockets structure will be possible. Inkjet printing has also the capability to produce different shapes and structures in order to alter trajectory behavior. As such we hope this new concept for making small-scale motile structures will lead to significant progress toward emerging applications.

Figure 1a displays the process by which the micro-rockets are digitally manufactured through RIJ of structure forming silk inks and methanol (which triggers conformation change of the printed silk) onto a silicon substrate. The 2D distribution of material can be digitally defined for each deposited layer, and the final height of the structures is controlled by the number of layers deposited (Figure S2, Supporting Information, demonstrates the linear relationship between the height and number of layers deposited). Batch fabrication of the micro-rockets can therefore be readily achieved by printing micro-pillar arrays using appropriately doped inks. Here we demonstrate the printing of rod-shaped micro-rockets with nominally uniform, single droplet, diameters using a MicroFab "Drop on Demand" printer equipped with Jetlab software and four single nozzle print heads (60 μ m diameter) each attached to its own individual reservoir. Successful layer-by-layer deposition of the silk scaffold requires a droplet of methanol to be deposited between each successive silk layer triggering the beta-sheet structure formation within the silk scaffold. In fact, to produce "Janus" micro-rockets with catalytically active and inactive parts, three different inks were sequentially deposited in this fashion: Ink A regenerated silk fibroin (RSF) mixed with catalase and polyethylene glycol (PEG₄₀₀, (average molecular number 400)), Ink B polymethyl methacrylate (PMMA) dissolved in dimethylformamide (DMF), and finally Ink C RSF mixed with PEG₄₀₀. Silk inks with concentration of 30 mg mL⁻¹ were used and resulted in an \approx 100 μ m diameter final structure for a single droplet as shown in Figure 1c. This final diameter is consistent with other published work

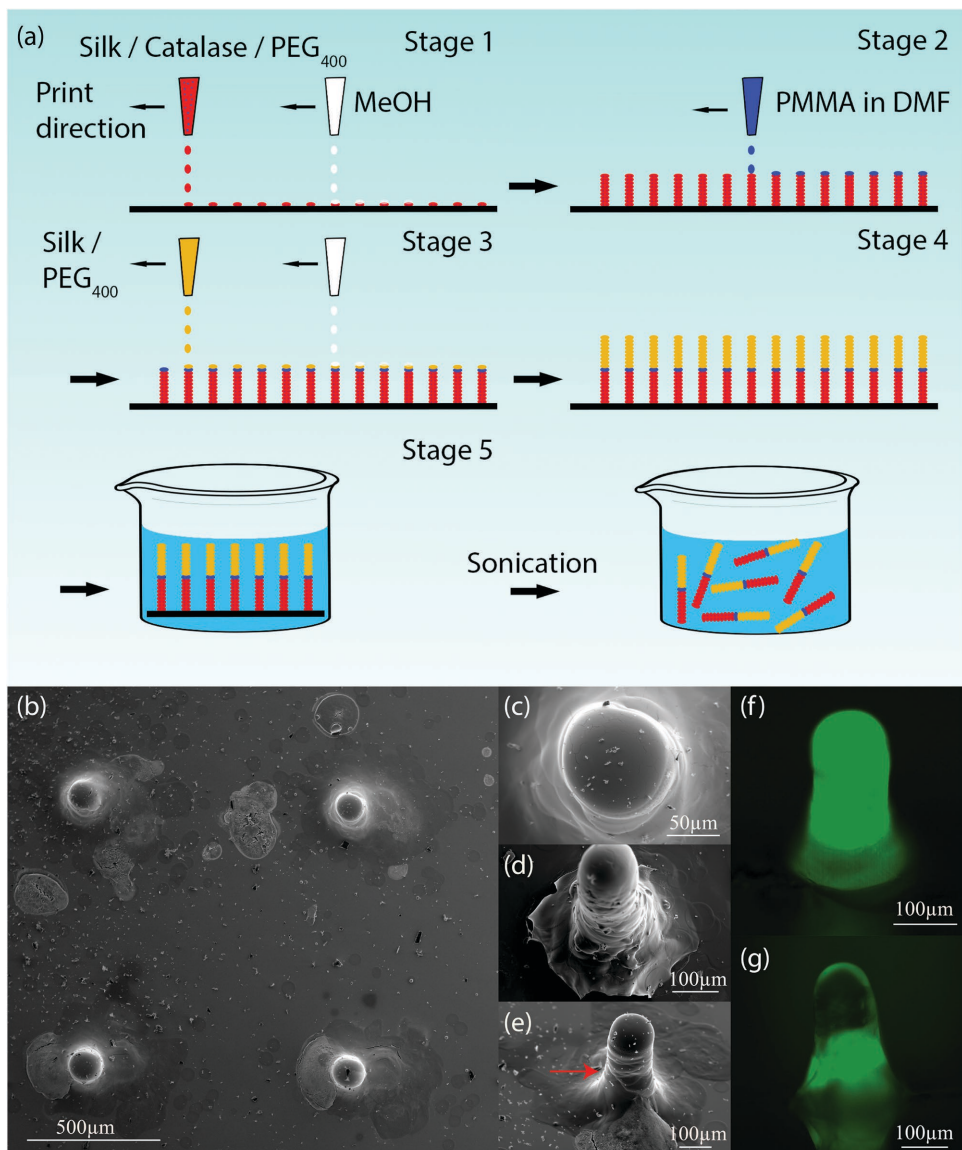


Figure 1. a) Schematic of the RIJ process for manufacturing catalytic micro-rockets. Stage 1: Alternate printing of a silk/catalase/PEG ink and a methanol ink (to transform printed silk ink from soluble random coils to insoluble beta-sheet structure) to build the catalytically active base of the micro-rocket. Stage 2: Ten layers of PMMA ink are deposited to act as a divider between the two halves of the rocket (to stop the penetration of oxygen bubbles generated into the inactive part of the micro-rocket). Stage 3: The second half of the rocket is deposited as in stage 1, but a silk/PEG ink is now used. Stage 4: Manufacture complete, substrate is immersed into the fluidic swimming media. Stage 5: Ultrasonication is used to detach the micro-rockets from the substrate. SEM images for micro-rockets: b) overview of silk rocket RIJ array, c) top view of a symmetrically active silk rocket, d) symmetrically active rocket, and e) Janus micro-rocket: red arrow indicates PMMA barrier layer between catalytically active and inactive segments; fluorescent microscopy images of FITC labeled catalase in micro-rockets: f) single ink micro-rocket (symmetrical) and g) Janus micro-rocket.

using silk inks which indicate diameters of 70–100 μm .^[34] PEG₄₀₀ was blended into the silk inks to enhance bubble detachment from the micro-rockets. (See Movie S6 without PEG₄₀₀, Supporting Information.) PEG is an FDA approved biocompatible material with stealth behavior.^[43] The two silk segments (colored in yellow and red in Figure 1a) were printed in equal numbers of layers (250), with ten layers of PMMA deposited in between to serve as a barrier layer to isolate the active and inactive halves. Figure 1 b–e shows scanning electron microscopy (SEM) images and fluorescent microscopy images of the resulting micro-rocket structures. Figure 1b shows the SEM image of the micro-rocket array fabricated through RIJ. Oblique observation (Figure 1d–g)

reveals that some widening at the base of the printed structures has occurred, leading to a conical “rocket” shape, despite the constant single droplet width defined in the digital design. This base widening probably indicates that upper layer inks to some extent flow down along the side of the micro-rocket. In order to demonstrate the ability to vary the composition of the micro-rockets while maintaining a given shape, and also to investigate the effect of the catalyst distribution on rocket motion, a fully active micro-rocket was also printed with an equivalent structure using only ink A (RSF, catalase, and PEG₄₀₀). SEM images revealed that this micro-rocket also had a similar 3D appearance (Figure 1d). In order to show the enzyme distribution in the fully active

and Janus rockets, fluorescein isothiocyanate (FITC) labeled catalase was used to allow fluorescent microscopy to directly reveal the enzyme distribution within the micro-rockets. A homogeneous enzyme distribution was observed for the fully active rocket (Figure 1f), while for the Janus rocket fluorescent labeled enzyme was observed only at the bottom half (Figure 1g).

Following manufacture, rockets were detached from the planar substrate using ultrasonication into the fluid of interest. Optical microscopy was used to confirm the equivalence of the final dimensions (the detached structures) of both the Janus and the fully active examples (Figure 2a,b).

To determine the effectiveness of Janus micro-rockets manufactured using RIJ, video microscopy was used to observe their motion when dispersed into an aqueous solution containing 5% wt/V hydrogen peroxide (Figure 2b and Movie S2, Supporting Information). It is clear that the catalase containing rear section of the rocket (Figure 1g) is causing decomposition of the dissolved hydrogen peroxide fuel at a sufficient rate to nucleate and grow oxygen bubbles, which detach and rapidly propel it forward via momentum transfer. Qualitatively, a strong link between the orientation of the printed device and the direction of motion is apparent, with motion proceeding away from the catalyst-containing segment (Figure 2a,b, Movies S1 and S2, Supporting Information). Note that the introduction of the PMMA barrier layer between the active and inactive segments is key to establish this behavior over long time periods. Without a barrier layer, large, slowly growing oxygen bubbles could also nucleate at the leading inactive end of the micro-rocket, and occasionally detach, causing the device to move in the opposite direction (see Movie S3, Supporting Information). This is thought to be due to porosity within the silk scaffold allowing oxygen generated by the catalase to reach all surfaces of the device.^[44] In order to further analyze the directional behavior of these Janus micro-rockets, the x and y coordinates for points at the front and back of a given device were manually tracked for each video frame. This allows the degree of correlation between the angle of orientation of the device (ϕ) and the subsequent angle of direction of travel (θ) to be compared (Figure 2c).^[45] Figure 2g overlays these two angles for a Janus micro-rocket, and confirms there is a strong correlation between device orientation and direction of travel. Figure 2f shows the same data, but for a homogenous, non-compartmentalized micro-rocket with catalase throughout the structure. In contrast, no correlation between orientation and subsequent direction of motion of these fully active micro-rockets is observed. This is presumably due to bubble release occurring stochastically from all regions of the device (Figure 2a, Movie S1, Supporting Information), as previously discussed and modeled for a simple spherical bubble propulsive particle.^[10] Similar analysis of 20 trajectories for micro-rockets with the two printed structures confirms that the correlation between device orientation and motion direction is strong for Janus micro-rockets ($r^2 = 0.656 \pm 0.023$ correlation coefficient) and weak for fully active micro-rockets ($r^2 = 0.003 \pm 0.017$ correlation coefficient).

Figure 2d,e compares trajectories for fully active and Janus micro-rockets. It is apparent that fully active rocket trajectories show frequent changes in direction, whereas the Janus micro-rockets exhibit greater directionality and persistent motion (persistence lengths calculated as described in Gregory et al.^[10]: Janus micro-rockets: $420 \pm 180 \mu\text{m}$, fully active micro-rockets: $25 \pm 6 \mu\text{m}$). The Janus micro-rockets also produce larger translation speeds ($510 \pm 90 \mu\text{m s}^{-1}$), compared to fully active devices ($370 \pm 20 \mu\text{m s}^{-1}$), despite the later having double the catalase content. This is likely due to the increased frequency of simultaneous bubble detachment from opposing surfaces for the fully active structures, which produce little net translation.^[10] These results clearly show the ability to use a digital manufacturing method to control catalyst distribution within a printed swimming device. In turn, this approach opens up a new route to easily control trajectories for specific intended micro-rocket applications, particularly if combined with shape modification as well.

To further assess the capabilities of these RIJ micro-rockets, we have surveyed previously published examples of bubble propulsive devices, Table 1. We discuss our results in the context of two key performance properties: velocity and solution constraints/biocompatibility. To start with, comparing our measured velocities with other self-motile devices, the RIJ rockets are well within the high speed region. Next, we consider solution requirements, including the ability to produce motion within biological fluids. Because microjets rely on fuel ingress into a tubular structure, these examples are highly sensitive to surface tension and need the addition of surfactants in order to decrease the surface tension and allow fuel ingress.^[14,46–54] Likewise, the majority of the reported spherical micromotors either need addition of a surfactant in order to achieve propulsion,^[6,7,10,55,56] or alternatively propulsion has only been demonstrated in a specific non-aqueous solvent system. For some of these examples, biocompatibility was also specifically assessed by measuring motion within fluids such as serum, and again surfactants were required in order for motion to be produced. This general requirement for the addition of a surfactant to the fluid to confer biocompatibility is highly undesirable, as it is well known to alter the structure of many biological components, e.g., protein and lipid membrane structure.^[25] While some studies suggested that the addition of a surfactant to confer biocompatibility was solely required to reduce surface tension,^[24,57] it is in fact likely that a significant role of the surfactant is also to reduce the degree of bio-fouling of the active surface of the device due to unfolding of proteins via surfactants such as sodium dodecyl sulfate (SDS).^[25] We also tabulate the two recent examples of screen-printed motile devices^[18] and micro-scale continuous optical printed devices.^[19] One of these^[25] requires surfactant to produce motion in aqueous solutions, and neither example was tested within a biological fluid: it is probable their biocompatibility may be limited by reliance on platinum as the catalyst.

Based on our observations that RIJ micro-rockets with an enzyme rather than platinum catalyst show rapid motion in aqueous solutions without surfactant, we also deployed them within human serum solutions. Figure 3 displays the

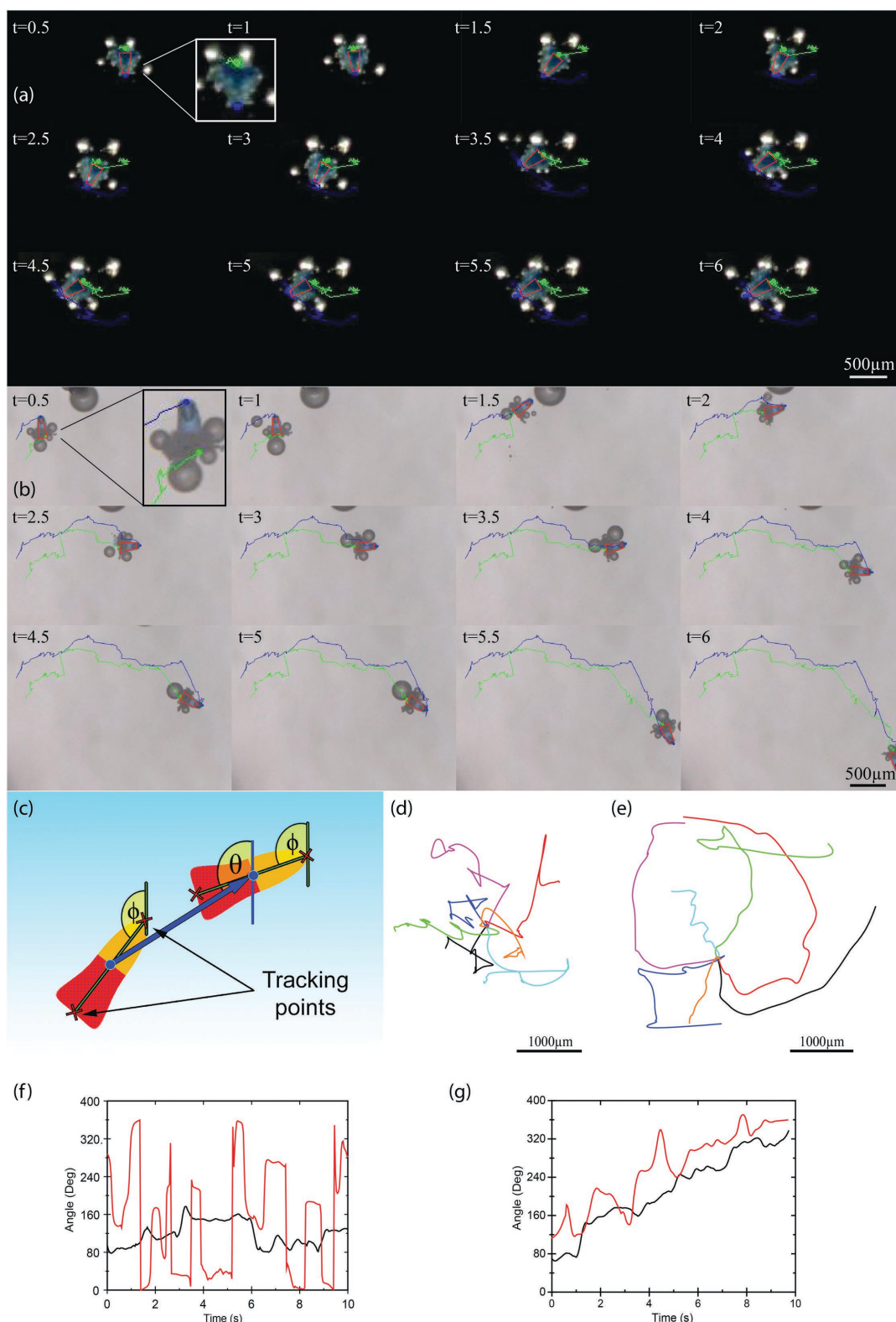


Figure 2. Still video frames from micro-rockets in 5% wt/V aqueous hydrogen peroxide solution for a) fully active and b) Janus, insets are zoomed in images of the rockets (Movies S1 and S2, Supporting Information). Red shape indicates approximate rocket orientation, for the Janus rocket blue line indicates trajectory for the catalytically active back end of the micro-rocket, green line indicates trajectory for the inactive front end of the micro-rocket. c) Schematic defining the angles determined from these trajectories and used for subsequent analysis. Trajectories (duration ≈ 10 s) for d) fully active and e) Janus micro-rockets. f) Representative graph of θ (black) and ϕ (red) angles over time for a fully active micro-rocket; g) representative plot of θ (black) and ϕ (red) angles for a Janus micro-rocket. Here, θ is the angle of the direction of travel, while ϕ is the angle of the orientation of the device. This result demonstrated that Janus micro-rockets have a high correlation ($r^2 = 0.656 \pm 0.023$) to their trajectory direction and fully active micro-rockets have a very weak correlation coefficient ($r^2 = 0.003 \pm 0.017$).

Table 1. Comparison of different swimming devices in various media.

Authors	Type of device	Surfactant	Velocity	Medium/fuel
Gregory et al. (this paper)	Silk/PEG/catalase fully active micro-rockets	No	370 $\mu\text{m s}^{-1}$	5% H_2O_2
	Silk/PEG/catalase Janus micro-rockets		510 $\mu\text{m s}^{-1}$	
	Silk/PEG/catalase fully active micro-rockets	No	282 $\mu\text{m s}^{-1}$	3% H_2O_2 in 2% human serum
	Silk/PEG/catalase Janus micro-rockets		338 $\mu\text{m s}^{-1}$	
Wang and co-workers ^[14]	PEDOT/Au-catalase (microjets)	Yes	120 $\mu\text{m s}^{-1}$	2% H_2O_2
Vicario et al. ^[55]	SiO_2 /synthetic manganese catalase	No	35 $\mu\text{m s}^{-1}$	5% H_2O_2 in CH_3CN /glycerol
Wang and co-workers ^[46]	PEDOT/PEDOT-COOH/Ni/Pt (microjets)	Yes	88 $\mu\text{m s}^{-1}$	1% H_2O_2 in PBS buffer
Wang and co-workers ^[47]	PAPBA/Pt (microjets)	Yes	40 $\mu\text{m s}^{-1}$	5% H_2O_2 in human serum
Wang and co-workers ^[48]	Ti/Fe/Au/Pt (microjets)	Yes	85 $\mu\text{m s}^{-1}$	7.5% H_2O_2 in human serum (1:4 diluted)
Wang and co-workers ^[49]	Ti/Ni/Au/Pt (microjets)	Yes	125 $\mu\text{m s}^{-1}$	3% H_2O_2 in protein solutions
Wang and co-workers ^[50]	PANI/Pt (microjets)	Yes	1.4 mm s^{-1}	5% H_2O_2
Pumera and co-workers ^[51]	Cu/Pt (microjets)	Yes	365 $\mu\text{m s}^{-1}$	3% H_2O_2
Sanchez et al. ^[52]	Ti/Fe/Pt (microjets)	Yes	130 $\mu\text{m s}^{-1}$	4% H_2O_2 in 25% cell medium
Sanchez et al. ^[53]	Ti/Cr/Pt (microjets)	Yes	500 $\mu\text{m s}^{-1}$	1% H_2O_2
Solovev et al. ^[54]	Ti/Fe/Pt (microjets)	Yes	220 $\mu\text{m s}^{-1}$	7.5% H_2O_2
Gregory et al. ^[10]	PS/Pt (spheres)	No	1.8 mm s^{-1}	2% H_2O_2
Wang and co-workers ^[56]	Al/Ga (Janus spheres)	Yes	3 mm s^{-1}	Water
Wang and co-workers ^[7]	TiO_2 /Au/Mg (spherical micromotors)	Yes	80 $\mu\text{m s}^{-1}$ 120 $\mu\text{m s}^{-1}$	Water seawater
Wang and co-workers ^[6]	Mg/Ti/Ni/Au (Janus spheres)	Yes	90 $\mu\text{m s}^{-1}$	Seawater
Kumar et al. ^[18]	Carbon/acrylic/Pt (catalytic fish ≈ 1 cm)	Yes	175 mm s^{-1}	15% H_2O_2
Zhu et al. ^[19]	PEGDA/Pt. nanoparticles (optical printed microfish)	NA	780 $\mu\text{m s}^{-1}$	15% H_2O_2

motion for a typical fully active (Figure 3a, Movie S4, Supporting Information) and a Janus (Figure 3b, Movie S5, Supporting Information) micro-rocket moving within a dilute serum solution (2% wt/V), doped only with 3% H_2O_2 fuel. It is clear that both devices can produce rapid motion in this biological solution without the addition of surfactant additives (mean velocity of fully active micro-rocket = 282 $\mu\text{m s}^{-1}$, Janus micro-rocket = 338 $\mu\text{m s}^{-1}$). The increased bubble generation observed for these devices operating within serum has affected their persistence of motion; however, the

Janus rockets still show improved directionality compared to homogeneously active devices (Movies S4 and S5, Supporting Information). Qualitatively, motion was observed to continue for more than 30 min, showing that the enzyme contained within the silk matrix was stably encapsulated. The micro-rockets were also tested in 0.1 M PBS solution (pH 7.4) and 0.2 M sodium carbonate (Na_2CO_3) (pH 10.0) with 3% H_2O_2 fuel, in both cases the rockets produced similar propulsion phenomenon. The solutions tested here span a pH range of 4–10, and this range appears to be appropriate

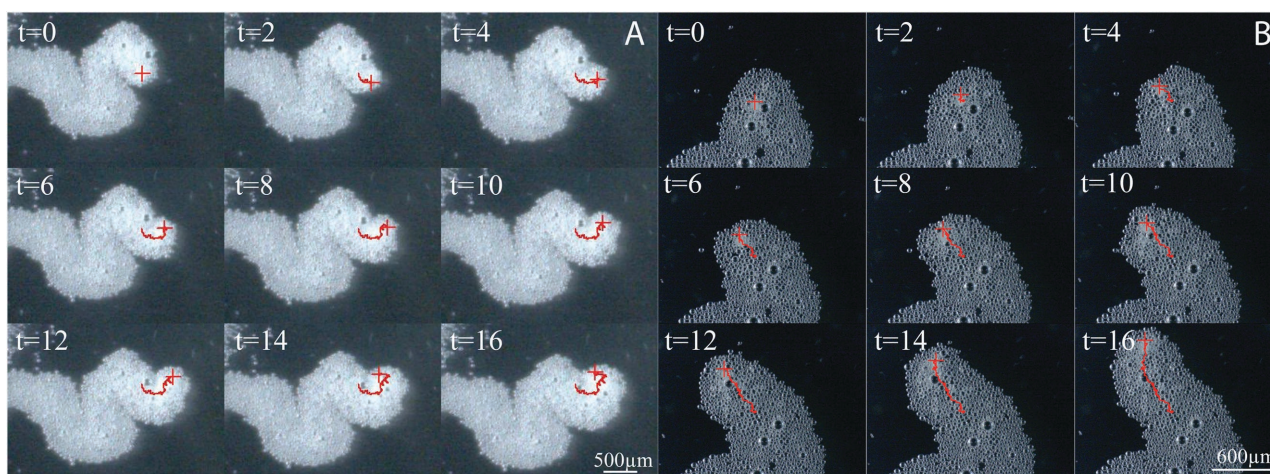


Figure 3. Still frames for A) a fully active and B) a Janus micro-rocket in 2% human serum solution containing 3% wt/V aqueous hydrogen peroxide fuel. Red lines indicate trajectories (Movies S4 and S5, Supporting Information).

for optimal performance. In the context of the above discussion, it appears that unlike the metallic catalyst powered devices, the silk/catalase-based micro-rockets developed here do not have any notable reaction rate inhibition due to biofouling. One of the chief emerging applications for self-motile materials is to aid lab-on-a-chip detection for biological analyses; this elimination of a potentially destructive additive represents a significant step forward.

The continued catalase reactivity even in low pH solutions of the silk rockets suggests that the catalytic activity is being preserved by the silk scaffold. Indeed, the enhanced stability of catalase and a variety of enzymes immobilized within a crystalline silk (Silk II) scaffold was reported by Lu et al.^[37] The observation of a similar effect here could suggest that catalytic reaction is occurring at both the surface and inside the micro-rocket. Evidence of this potential for product and reagent diffusion within the device is also supplied by the observation of growing bubbles at the inactive surfaces of Janus micro-rockets when the two segments were not separated by a PMMA barrier layer (Movie S3, Supporting Information).

In summary, here we have shown a new approach to producing self-motile micro-rockets based on RIJ of a silk scaffold doped with catalase and PEG₄₀₀. This approach allows the distribution of catalyst to be varied at will, and here we used this to demonstrate that rockets with asymmetric distributions of catalyst produce faster more directional motion, compared to those with uniform activity, due to unopposed stochastic bubble release. The potential to expand upon this initial demonstration is great, not least due to the large number of materials (e.g., drugs, enzymes, and antibodies) that can be encapsulated within the silk scaffold.^[33,34,38,42,58] This will, for example, in the future allow straightforward investigations of new enzymatic reactions not reliant on peroxide fuel to power devices, addition of selective cargo binding chemistry to the inactive segment, and incorporation of magnetic materials to allow steering by external fields. We also note that RIJ technology is subject to rapid development, which will open up the potential to further miniaturize devices. Although resolution is dependent on material properties, currently structures as small as 10 μm have been reported using RIJ.^[21]

Supporting Information

Supporting Information is available from the Wiley Online Library or from the author.

Acknowledgements

The authors would like to acknowledge support from the EPSRC via X. Zhao's reactive inkjet printing of silk materials awards (EP/N007174/1 and EP/N023579/1), S. J. Ebbens Career Acceleration Fellowship (EP/I002402/1), and P. J. Smith's reactive inkjet printing award (EP/I014850/1).

- [1] a) M. Leoni, J. Kotar, B. Bassetti, P. Cicuta, M. C. Lagomarsino, *Soft Matter* **2009**, *5*, 472; b) A. Najafi, R. Golestanian, *J. Phys.: Condens. Mater.* **2005**, *17*, S1203.
- [2] a) S. Dühr, D. Braun, *Proc. Natl. Acad. Sci. USA* **2006**, *103*, 19678; b) F. Julicher, J. Prost, *Eur. Phys. J. E* **2009**, *29*, 27.
- [3] S. Ebbens, D. A. Gregory, G. Dunderdale, J. R. Howse, Y. Ibrahim, T. B. Liverpool, R. Golestanian, *EPL* **2014**, *106*, 58003.
- [4] S. J. Ebbens, *Curr. Opin. Colloid Interface Sci.* **2015**, *21*, 14.
- [5] a) L. Soler, S. Sanchez, *Nanoscale* **2014**, *6*, 7175; b) L. Soler, V. Magdanz, V. M. Fomin, S. Sanchez, O. G. Schmidt, *ACS Nano* **2013**, *7*, 9611; c) J. Orozco, G. Cheng, D. Vilela, S. Sattayasamitsathit, R. Vazquez-Duhalt, G. Valdes-Ramirez, O. S. Pak, A. Escarpa, C. Kan, J. Wang, *Angew. Chem., Int. Ed.* **2013**, *52*, 13276.
- [6] W. Gao, X. Feng, A. Pei, Y. Gu, J. Li, J. Wang, *Nanoscale* **2013**, *5*, 4696.
- [7] J. Li, V. V. Singh, S. Sattayasamitsathit, J. Orozco, K. Kaufmann, R. Dong, W. Gao, B. Jurado-Sanchez, Y. Fedorak, J. Wang, *ACS Nano* **2014**, *8*, 11118.
- [8] Z. Ghalanbor, S. A. Marashi, B. Ranjbar, *Med. Hypotheses* **2005**, *65*, 198.
- [9] L. Baraban, D. Makarov, R. Streubel, I. Mönch, D. Grimm, S. Sanchez, O. G. Schmidt, *ACS Nano* **2012**, *6*, 3383.
- [10] D. A. Gregory, A. I. Campbell, S. J. Ebbens, *J. Phys. Chem. C* **2015**, *119*, 15339.
- [11] a) J. R. Howse, R. A. L. Jones, A. J. Ryan, T. Gough, R. Vafabakhsh, R. Golestanian, *Phys. Rev. Lett.* **2007**, *99*; b) S. Ebbens, M. H. Tu, J. R. Howse, R. Golestanian, *Phys. Rev. E* **2012**, *85*; c) S. J. Ebbens, G. A. Buxton, A. Alexeev, A. Sadeghi, J. R. Howse, *Soft Matter* **2012**, *8*, 3077; d) R. Golestanian, T. B. Liverpool, A. Ajdari, *Phys. Rev. Lett.* **2005**, *94*.
- [12] a) J. G. Gibbs, Y. P. Zhao, *Appl. Phys. Lett.* **2009**, *94*; b) L. Li, J. Wang, T. Li, W. Song, G. Zhang, *Soft Matter* **2014**, *10*, 7511; c) V. M. Fomin, M. Hippler, V. Magdanz, L. Soler, S. Sanchez, O. G. Schmidt, *IEEE Trans. Rob.* **2014**, *30*, 40.
- [13] R. J. Archer, A. I. Campbell, S. J. Ebbens, *Soft Matter* **2015**, *11*, 6872.
- [14] J. Orozco, V. Garcia-Gradilla, M. D'Agostino, W. Gao, A. Cortes, J. Wang, *ACS Nano* **2013**, *7*, 818.
- [15] D. Pantarotto, W. R. Browne, B. L. Feringa, *Chem. Comm.* **2008**, 1533.
- [16] S. Sengupta, D. Patra, I. Ortiz-Rivera, A. Agrawal, S. Shklyae, K. K. Dey, U. Cordova-Figueroa, T. E. Mallouk, A. Sen, *Nat. Chem.* **2014**, *6*, 415.
- [17] a) L. K. E. A. Abdelmohsen, M. Nijemeisland, G. M. Pawar, G.-J. A. Janssen, R. J. M. Nolte, J. C. M. van Hest, D. A. Wilson, *ACS Nano* **2016**, *10*, 2652; b) X. Ma, X. Wang, K. Hahn, S. Sanchez, *ACS Nano* **2016**, *10*, 3597; c) X. Ma, A. Jannasch, U.-R. Albrecht, K. Hahn, A. Miguel-Lopez, E. Schaeffer, S. Sanchez, *Nano Lett.* **2015**, *15*, 7043; d) Z. Wu, X. Lin, T. Si, Q. He, *Small* **2016**.
- [18] R. Kumar, M. Kiristi, F. Soto, J. Li, V. V. Singh, J. Wang, *RSC Adv.* **2015**, *5*, 78986.
- [19] W. Zhu, J. Li, Y. J. Leong, I. Rozen, X. Qu, R. Dong, Z. Wu, W. Gao, P. H. Chung, J. Wang, S. Chen, *Adv. Mater.* **2015**, *27*, 4411.
- [20] H. Meier, U. Loeffelmann, D. Mager, P. J. Smith, J. G. Korvink, *Phys. Status Solidi A* **2009**, *206*, 1626.
- [21] C. E. Hendriks, P. J. Smith, J. Perelaer, A. M. J. Van den Berg, U. S. Schubert, *Adv. Funct. Mater.* **2008**, *18*, 1031.
- [22] Z. Y. Li, P. Beck, D. A. A. Ohlberg, D. R. Stewart, R. S. Williams, *Surf. Sci.* **2003**, *529*, 410.
- [23] G. Zhao, S. Sanchez, O. G. Schmidt, M. Pumera, *Nanoscale* **2013**, *5*, 2909.
- [24] H. Wang, G. Zhao, M. Pumera, *J. Phys. Chem. C* **2014**, *118*, 5268.
- [25] S. Ghosh, S. Chakrabarty, D. Bhowmik, G. S. Kumar, N. Chattopadhyay, *J. Phys. Chem. B* **2015**, *119*, 2090.
- [26] P. J. Smith, A. Morrin, *J. Mater. Chem.* **2012**, *22*, 10965.

- [27] B. B. Mandal, A. Grinberg, E. S. Gil, B. Panilaitis, D. L. Kaplan, *Proc. Natl. Acad. Sci. USA* **2012**, *109*, 7699.
- [28] B. Kundu, R. Rajkhowa, S. C. Kundu, X. Wang, *Adv. Drug Delivery Rev.* **2013**, *65*, 457.
- [29] H. J. Jin, J. Park, V. Karageorgiou, U. J. Kim, R. Valluzzi, D. L. Kaplan, *Adv. Funct. Mater.* **2005**, *15*, 1241.
- [30] D. N. Rockwood, R. C. Preda, T. Yucel, X. Wang, M. L. Lovett, D. L. Kaplan, *Nat. Protoc.* **2011**, *6*, 1612.
- [31] C. Vepari, D. L. Kaplan, *Prog. Polym. Sci.* **2007**, *32*, 991.
- [32] a) H. J. Jin, D. L. Kaplan, *Nature* **2003**, *424*, 1057; b) A. Motta, L. Fambri, C. Migliarese, *Macromol. Chem. Phys.* **2002**, *203*, 1658.
- [33] H. Tao, B. Marelli, M. Yang, B. An, M. S. Onses, J. A. Rogers, D. L. Kaplan, F. G. Omenetto, *Adv. Mater.* **2015**, *27*, 4273.
- [34] R. Suntivich, I. Drachuk, R. Calabrese, D. L. Kaplan, V. V. Tsukruk, *Biomacromolecules* **2014**, *15*, 1428.
- [35] a) X. Y. Zhang, Y. D. Zhang, *Cell Biochem. Biophys.* **2015**, *72*, 777; b) A. M. J. van den Berg, P. J. Smith, J. Perelaer, W. Schrof, S. Koltzenburg, U. S. Schubert, *Soft Matter* **2007**, *3*, 238; c) A. M. J. van den Berg, A. W. M. de Laat, P. J. Smith, J. Perelaer, U. S. Schubert, *J. Mater. Chem.* **2007**, *17*, 677.
- [36] G. H. Altman, F. Diaz, C. Jakuba, T. Calabro, R. L. Horan, J. Chen, H. Lu, J. Richmond, D. L. Kaplan, *Biomaterials* **2003**, *24*, 401.
- [37] S. Z. Lu, X. Q. Wang, Q. Lu, X. Hu, N. Uppal, F. G. Omenetto, D. L. Kaplan, *Biomacromolecules* **2009**, *10*, 1032.
- [38] a) E. Wenk, A. J. Wandrey, H. P. Merkle, L. Meinel, *J. Controlled Release* **2008**, *132*, 26; b) K. Numata, D. L. Kaplan, *Adv. Drug Delivery Rev.* **2010**, *62*, 1497.
- [39] a) S. Hofmann, C. T. W. P. Foo, F. Rossetti, M. Textor, G. Vunjak-Novakovic, D. L. Kaplan, H. P. Merkle, L. Meinel, *J. Controlled Release* **2006**, *111*, 219; b) E. Wenk, H. P. Merkle, L. Meinel, *J. Controlled Release* **2011**, *150*, 128; c) K. Numata, B. Subramanian, H. A. Currie, D. L. Kaplan, *Biomaterials* **2009**, *30*, 5775.
- [40] a) H. Y. Wang, Y. Q. Zhang, *Soft Matter* **2013**, *9*, 138; b) K. Wei, I.-S. Kim, *Advances in Nanofibers*, (Ed: R. Maguire), InTech, Croatia, **2013**, 103. c) K. H. T. Thomas, T. Siew-Lok, C. H. G. James, *Biomed. Mater.* **2010**, *5*, 035008.
- [41] a) Y. Wang, D. D. Rudym, A. Walsh, L. Abrahamsen, H.-J. Kim, H. S. Kim, C. Kirker-Head, D. L. Kaplan, *Biomaterials* **2008**, *29*, 3415; b) L. Zhang, X. Cao, L. Wang, X. Zhao, S. Zhang, P. Wang, *Analyst* **2015**, *140*, 4105.
- [42] Y. Q. Zhang, *Biotechnol. Adv.* **1998**, *16*, 961.
- [43] K. Knop, R. Hoogenboom, D. Fischer, U. S. Schubert, *Angew. Chem., Int. Ed.* **2010**, *49*, 6288.
- [44] a) N. Minoura, M. Tsukada, M. Nagura, *Polymer* **1990**, *31*, 265; b) H. J. Kim, U.-J. Kim, G. Vunjak-Novakovic, B.-H. Min, D. L. Kaplan, *Biomaterials* **2005**, *26*, 4442.
- [45] S. J. Ebbens, J. R. Howse, *Langmuir* **2011**, *27*, 12293.
- [46] M. Garcia, J. Orozco, M. Guix, W. Gao, S. Sattayasamitsathit, A. Escarpa, A. Merkoci, J. Wang, *Nanoscale* **2013**, *5*, 1325.
- [47] F. Kuralay, S. Sattayasamitsathit, W. Gao, A. Uygun, A. Katzenberg, J. Wang, *J. Am. Chem. Soc.* **2012**, *134*, 15217.
- [48] S. Balasubramanian, D. Kagan, C.-M. J. Hu, S. Campuzano, M. J. Lobo-Castanon, N. Lim, D. Y. Kang, M. Zimmerman, L. Zhang, J. Wang, *Angew. Chem., Int. Ed.* **2011**, *50*, 4161.
- [49] J. Orozco, S. Campuzano, D. Kagan, M. Zhou, W. Gao, J. Wang, *Anal. Chem.* **2011**, *83*, 7962.
- [50] W. Gao, S. Sattayasamitsathit, J. Orozco, J. Wang, *J. Am. Chem. Soc.* **2011**, *133*, 11862.
- [51] W. Gao, S. Sattayasamitsathit, J. Orozco, J. Wang, *Nanoscale* **2013**, *5*, 8909.
- [52] S. Sanchez, A. A. Solovev, S. Schulze, O. G. Schmidt, *Chem. Commun.* **2011**, *47*, 698.
- [53] S. Sanchez, A. N. Ananth, V. M. Fomin, M. Viehrig, O. G. Schmidt, *J. Am. Chem. Soc.* **2011**, *133*, 14860.
- [54] A. A. Solovev, S. Sanchez, M. Pumera, Y. F. Mei, O. G. Schmidt, *Adv. Funct. Mater.* **2010**, *20*, 2430.
- [55] J. Vicario, R. Eelkema, W. R. Browne, A. Meetsma, R. M. La Crois, B. L. Feringa, *Chem. Commun.* **2005**, 3936.
- [56] W. Gao, A. Pei, J. Wang, *ACS Nano* **2012**, *6*, 8432.
- [57] J. Simmchen, V. Magdanz, S. Sanchez, S. Chokmaviroj, D. Ruiz-Molina, A. Baeza, O. G. Schmidt, *RSC Adv.* **2014**, *4*, 20334.
- [58] a) P. Wang, C. Qi, Y. Yu, J. Yuan, L. Cui, G. Tang, Q. Wang, X. Fan, *Appl. Biochem. Biotechnol.* **2015**, *177*, 472; b) C. P. Vepari, D. L. Kaplan, *Biotechnol. Bioeng.* **2006**, *93*, 1130; c) X. Wang, E. Wenk, A. Matsumoto, L. Meinel, C. Li, D. L. Kaplan, *J. Controlled Release* **2007**, *117*, 360.

Received: March 17, 2016
 Revised: April 25, 2016
 Published online: